A. Tomala[a], I. C. Gebeshuber[a,b], A. Pauschitz[c], M. Roy[d]
[a] Institute of Applied Physics, Vienna University of Technology, 1040 Wien, Austria
[b] Institute of Microengineering and Nanoelectronics, Universiti Kebangsaan Malaysia, 43600 UKM Bangi, Malaysia
[c] Austrian Center of Competence for Tribology, Wiener Neustadt, Austria
[d] Defence Metallurgical Research Laboratory,
PO: Kanchanbagh, Hyderabad, India

A comparative AFM study of carbon alloyed Mo–Se–C and W–S–C films for tribological applications

Transition metal dichalcogenides have a layered structure and are therefore promising self-lubricating films. They can be considered as potential substitutes for carbon based films in various environmental conditions. In this work, a comparative atomic force microscopy study of co-sputtered Mo–Se–C and W–S–C films is performed to evaluate their nanotribological performances. Both films are alloyed with carbon. The microstructural features of these films are characterised using scanning electron microscopy and X-ray diffraction. The hardness and elastic modulus of these films are measured employing nanoindentation. The topography, friction forces and pull off forces of the films are evaluated by means of atomic force microscopy and force spectroscopy. The results show that the roughness parameters of Mo–Se–C films are lower than that of W–S–C films at high carbon content whereas the reverse is true at low carbon content. Adhesion forces of these films based on pull-off force measurements show that Mo–Se–C films have higher pull off forces than W–S–C films. An atomic force microscopy technique is developed to estimate microscopic values of friction coefficients and to characterise the nature of surface changes due to nanotribological experiments. The friction coefficient of Mo–Se–C films is higher than that of W–S–C films at low carbon content and these friction coefficients are comparable at high carbon content.

Keywords: Transition metal dichalcogenides; Nanotribology; AFM study

1. Introduction

Transition metal dichalcogenides (TMD) are self-lubricating films having promising application in demanding environments such as vacuum and at medium temperature (up to 200 °C). These films can be considered important for many applications such as in micro electro-mechanical systems (MEMS) and micro mechanical assembly (MMA) requiring very low applied force. Micro/nanotribological studies are needed to understand the phenomena on a small scale. Probe-based microscopes (e. g. atomic force microscope (AFM)) and the surface force apparatus are widely used for this purpose.

Homogeneous TMD films can be obtained by direct current (DC) sputtering, DC magnetron sputtering, magnetron sputtering, bipolar pulsed magnetron sputtering and radio frequency (RF) sputtering [1–4] etc. These films can also be obtained by pulse laser deposition [5]. Magnetron sputtering is one of the most convenient methods as it allows easy alloying of TMD with other elements.

Among the TMD family, only MoS_2 and to some extent WS_2 have been studied systematically, while other candidates, such as selenides or tellurides, stood partially aside. It has been shown that molybdenum diselenide is much less sensitive to air humidity than the corresponding sulphide [6, 7]. It was also noted that WS_2 co-sputtered with carbon significantly improves tribological properties compared to pure WS_2 [8, 9]. Furthermore the best combination of mechanical and tribological properties was obtained for TMD alloyed with carbon at around 50 at.% C [10]. Thus the objective of the present work is to carry out a comparative AFM investigation of co-sputtered Mo–Se–C and W–S–C films keeping nanotribological application in mind. It should be stated that both varieties of films contain around 35 at.% and 50 at.% carbon.

2. Experimental details

2.1. Deposition of the film

All coatings were deposited on 100Cr6 polished steel samples, with hardness varying between 1.5 and 9.5 GPa. Coatings were deposited by r.f. magnetron sputtering of a carbon target with pellets of $MoSe_2$ in a basic ESM 100 Edwards unit in an argon atmosphere following a similar procedure as presented in previous research [10]. The pellets (99.8 % pure) with dimensions of $1.5 \times 3 \times 4\ mm^3$ were distributed uniformly in the circular erosion zone of the carbon target. Their number was varied between 16 and 72. For W–S–C films WS_2 pellets were used instead of $MoSe_2$ pellets. Before deposition, the substrates were cleaned for 30 min by establishing the plasma close to the substrate electrode. The discharge pressure and the power density were 0.75 Pa and $8\ W\ cm^{-2}$, respectively. The deposition time was 1 h giving rise to a final thickness of the coatings in the range of 1 μm to 3 μm. No substrate bias was applied during the deposition.

2.2. Structural characterisation of the films

The chemical composition and the cross-section morphologies of these films were analysed using a Cameca SX 50 electron probe microanalysis (EPMA) apparatus and a Jeol scanning electron microscope (SEM), respectively. X-ray diffraction patterns were obtained from the coated surfaces using a Philips PW 1830 diffractometer in glancing mode to examine the structure of these films. The X-ray diffractometer was set at 40 kV and 30 mA with radiation target Co-K_α and a nickel filter. The diffraction patterns were recorded at a speed of $0.01^\circ\ s^{-1}$.

2.3. Nanohardness measurement

The hardness and the elastic modulus of these films were determined with an indentation tester equipped with a Berkovich three-sided pyramidal diamond indenter with a nominal angle of 63.5°. The instrument was placed in a vibration free isolated chamber. The applied load was 2 mN. The load was selected so as to keep the deformation confined within the film. The load and displacement resolution of the instrument were 50 nN and 0.1 nm respectively. The holding time of indentation was 5 s in all cases. Both loading and unloading times were 10 s. The experimental results were corrected for the thermal drift of the equipment and for the uncertainty in the zero positions. The reported hardness and elastic modulus are averages of 10 indentations for each sample on different surface position separated by 50 µm. The elastic modulus was determined using the procedure proposed by Oliver and Pharr [11]. The nanoindenter was calibrated by indenting on a fused silica sample and measuring the hardness and elastic modulus of fused silica with hardness and elastic modulus approximately 10 and 73 GPa, respectively. Measurements were performed in a clean air environment with a relative humidity of approximately 40 % while the temperature was around 22 °C.

2.4. AFM measurement

AFM measurements were performed with an AFM MFP-3D atomic force microscope (Asylum Research, Santa Barbara, CA) in ambient conditions using non conductive silicon nitride cantilevers with spring constant $k = 0.1\ N^{-1}\ m$ and resonant frequency $f_0 = 26-50$ kHz (Veeco). The main measurement parameters were: scan size of 5 µm, scan rate 1 Hz, scan angle 90°, 512 scan points, 512 scan lines, and a set point of 10 nN in contact mode. The recorded data are height trace/retrace, deflection trace/retrace, and lateral trace/retrace. The parameters of cantilevers and triangular tips are given in Table 1. In the present investigation the lateral force technique was used for friction measurements. The sample was scanned perpendicularly to the long axis of the cantilever beam and the lateral force signals in trace and retrace (LT, LRT) modes were recorded. To obtain the friction force value (*FFV*), as introduced by Bhushan and co-workers two average values (Lateral Trace (LTV_{avg}) and Lateral Retrace ($LRTV_{avg}$) from every scan) have to be subtracted from each other, and the subtracted value is to be divided by two [12] employing eq. (1) as given below.

Table 1. Major features of the cantilever used for AFM study.

	Cantilever-1 (Topography & LFM)
Material	Si_3N_4
Cantilever spring constant	0.1 N m^{-1}
Cantilever arm length	140 µm
Cantilever arm width	18 µm
Resonance frequency	38 kHz
Full tip opening angle	35°
Tip radius	10 nm

$$FFV = \frac{|LTV_{avg} - LRTV_{avg}|}{2} \quad (1)$$

Assuming that the friction in nanoscale follows Amonton's law, the friction force is given by:

$$FFV = \mu(SP + F_0) \quad (2)$$

Where μ is the friction coefficient, *SP* (set point) is the applied load and F_0 is a force constant. Following the procedure suggested by Beake et al. [13] the force constant is nearly equal to the pull off force determined from the force distance curves. Thus,

$$\mu = \frac{FFV}{(SP + F_0)} \quad (3)$$

In order to obtain SI units (N, Newton), the lateral force needs to be calibrated with the slope of deflection vs. LVDT. After the calibration an accurate value of *InvOLS* (Inverse Optical Lever Sensitivity) was obtained. *InvOLS* is the sensitivity of the detector-cantilever combination. With an accurate value of *InvOLS* it is possible to calculate *FFV* and *SP* in Newton as given below.

FFV (V) · *InvOLS* (nm V^{-1}) · spring constant

(nN nm^{-1}) = (nN) (4)

SP (V) · *InvOLS* (nmV^{-1}) · spring constant

(nN nm^{-1}) = (nN) (5)

3. Results

The chemical compositions of all films are summarized in Table 2. Films denoted Mo series are Mo–Se–C whereas films in the W series are W–S–C. Films with low carbon (Mo1 and W1) contain around 35 at.% carbon and films with high carbon content (Mo2, W2) have around 50 at.% carbon. In addition to Mo, W, S, Se and C, contamination due to O_2 arising out of residual water vapour and the target

Table 2. Chemical compositions of the test materials.

Film Designation	at.% Mo	at.% W	at.% S	at.% Se	at.% C	at.% O_2
Mo1	21.7			38.6	36.9	2.8
W1		22.6	39.8		34.6	3.0
Mo2	16.5			29.7	48.5	5.4
W2		17.7	28.2		49.0	5.1

or from surface adsorption from the atmosphere after deposition was also detected. Lower chalchogen content in relation to the stoichiometry (S/W = 2) is related to preferential sputtering of S or Se by energetic species during deposition [2].

The XRD patterns of films W2 and Mo2 are illustrated in Fig. 1. Again, no significant changes are detected in relation to the previous work [9]. The main points worth mentioning are: domination of the XRD patterns by main broad asymmetric peaks which are indexed with the general form (10 L) corresponding to a turbostrating stacking of the family of planes (10 L) with $L = 0,1,2,3$ [14] of the hexagonal WS_2 phase (ICDD 84-1398). The XRD diffraction pattern of Mo–Se–C coatings shows a peak close to $2\theta \approx 37.5^\circ$ ($MoSe_2$ phase with (100) orientation) followed by a second peak at $2\theta \approx 44.5^\circ$. The latter is highly asymmetric with a long tail towards higher 2θ. Finally a last peak positioned at $2\theta \approx 70^\circ$ can be indexed as (110). Weise et al. [15] demonstrated that the extended shoulder of the sputtered MoS_2 peak positioned close to $2\theta \approx 40^\circ$ corresponded to a turbostrating stacking of (10 L) planes ($L = 0, 1, 2, 3$). Because of the similarity in the nature of the curves, XRD patterns of the W–S–C and Mo–Se–C films with low carbon content are not shown for the sake of brevity.

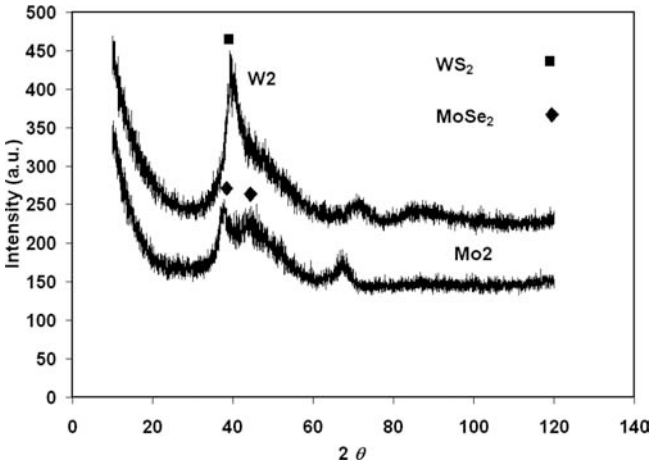

Fig. 1. XRD patterns of W–S–C film (W2) and Mo–Se–C film (Mo2).

Figure 2 shows the cross-section morphology of Mo–Se–C (films Mo1 and Mo2) W–S–C (film W1 and W2) coatings imaged using SEM. All the films exhibit a columnar structure. The microstructures of Mo–Se–C films are finer than the microstructures of W–S–C films. Further, W–S–C films have a tendency to become amorphous. The tendency to become amorphous increases with increasing carbon content. Further description in relation to characteristics of the films can be found elsewhere [16]. The thickness of W–S–C film varies between 1 μm to 2 μm whereas that of Mo–Se–C film varies between 2 μm and 3 μm.

The load vs. displacement curves of these films obtained at an applied load of 2 mN are illustrated in Fig. 3. Each curve is obtained by averaging ten different curves. All the curves are smooth and none of the curves shows the presence of pop-in or pop-out events, thus indicating no evidence of fracture of the film. It is clear that films with lower carbon content exhibit higher depth of penetration. The depth of indentation of W–S–C films is significantly lower than the depth of indentation of Mo–Se–C films. During the hold at the maximum load, the displacement increases in all the films indicating drift due to creep as the load vs. displacement curves are plotted after incorporating the correction due to thermal drift. The extent of this drift decreases with increasing carbon content for Mo–Se–C variety films. It is independent of carbon content for W–S–C film. It should be noted that the elastic modulus and the hardness have been determined for each individual curve although in Fig. 3 only averaged curves are presented. The average values of elastic modulus and hardness of the tested films determined from individual curves are given in Ta-

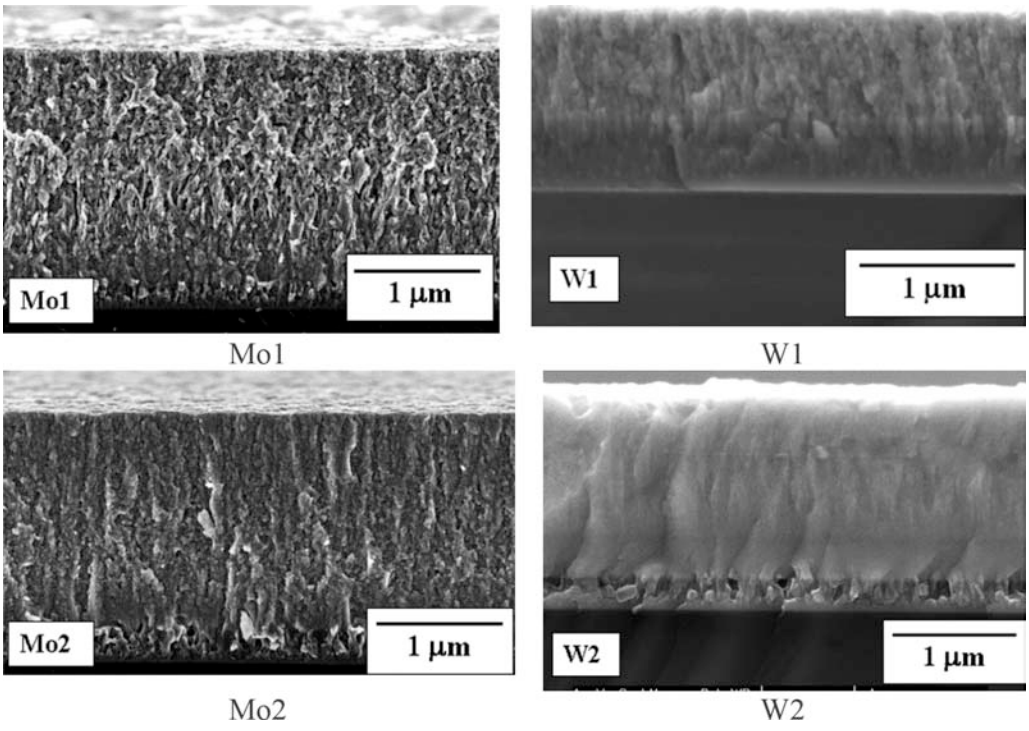

Fig. 2. Cross-section morphology of W–S–C (films W1, W2) and Mo–Se–C (films MO1, MO2) coatings imaged using SEM.

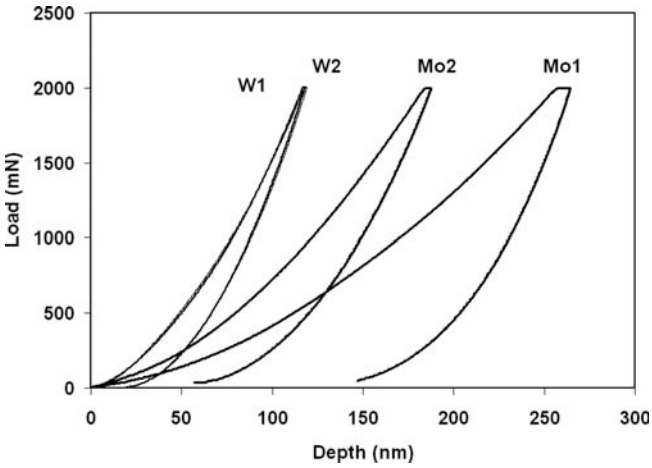

Fig. 3. Averaged load vs. displacement curves of the films investigated.

Table 3. Elastic modulus and hardness of the films investigated.

Film	*E* (GPa)	*SD*	*H* (GPa)	*SD*
Mo1	26.0	1.1	1.4	0.11
W1	73	9.9	9.1	2.0
Mo2	39.0	2.8	4.0	0.44
W2	74	2.1	9.4	0.51

Table 4. Roughness parameters of the investigated films. Image size 5 μm×5 μm.

Films	RMS (nm)	Average height (nm)	Maximum height (nm)
Mo1	26.6 ± 3.0	339.0 ± 41.0	113.9 ± 26.5
W1	18.2 ± 2.0	91.7 ± 9.0	84.4 ± 14.0
Mo2	27.0 ± 3.0	134.0 ± 13.0	94.5 ± 21.0
W2	29.8 ± 3.0	595.0 ± 60.0	117.1 ± 21.0

ble 3 along with their standard deviation. Clearly, the hardness and elastic modulus of W–S–C variety of films are significantly higher than these parameters of Mo–Se–C films. As expected, for each variety of film both elastic modulus and hardness increase with carbon content. The extent of increase of mechanical properties with the carbon content is more for Mo–Se–C films than W–S–C films. In other words, the carbon content has a negligible effect on the mechanical properties of W–S–C films.

Three dimensional AFM images showing the topographies of these films are illustrated in Fig. 4. Commensurate with the SEM micrographs, Mo–Se–C films have sharper peaks compared to W–S–C films. The peaks of W–S–C films are more rounded than the peaks of Mo–S–C films. It is also to be noted that the peaks tend to become blunt with the increase of carbon content for both variety of films. The important roughness parameters for tested films are listed in Table 4. Table 4 points on that roughness parameters such as RMS. (root mean square) average height, minimum height etc. are higher for Mo–Se–C films at low carbon content than W–S–C films and vice versa at high carbon content. In addition, the RMS value for both varieties of film increases with carbon content.

To understand the nature of the interaction between the cantilever tip and the coating, the deflection displacement curves were recorded. Figure 5 shows the deflection of the cantilever tip as a function of the distance from the film surfaces for all these films. In all cases, the darker line indicates tip approach to the surface and the dashed line represents the tip being pulled away from the surface. The vertical separation between the point where the tip touches the surface (denoted "A" in Fig. 5) and the point where the tip is pulled off the film (B) together with spring constant of the cantilever (0.1 nN nm^{-1}) are used to calculate the pull off (adhesive) force [12]. The pull of forces for film Mo1, Mo2, W1, and W2 are 26 nN (±3 nN), 18 nN (±2 nN), 10 nN (±1 nN) and 8 nN (±1 nN) respectively. It can clearly be seen that the pull off force decreases with increasing carbon content.

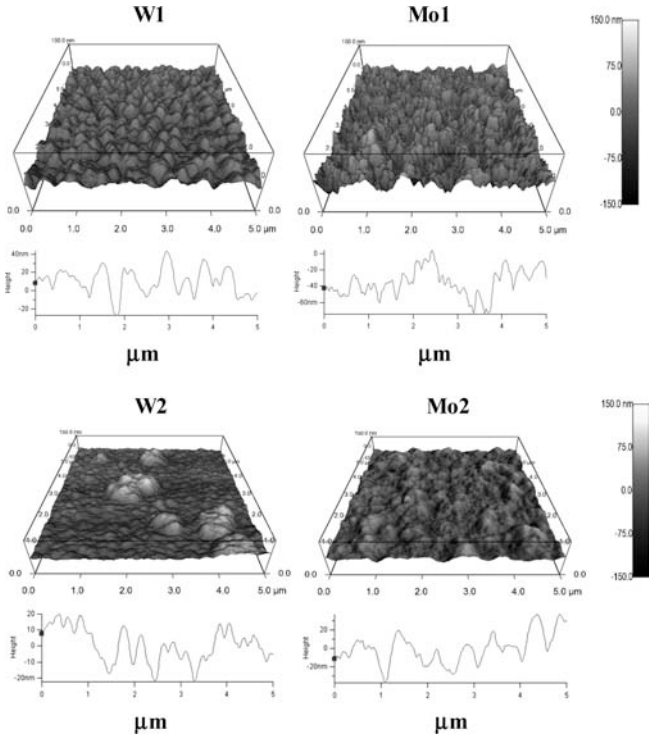

Fig. 4. Three-dimensional AFM images showing the topography of the investigated films together with representative cross-sectional line scans.

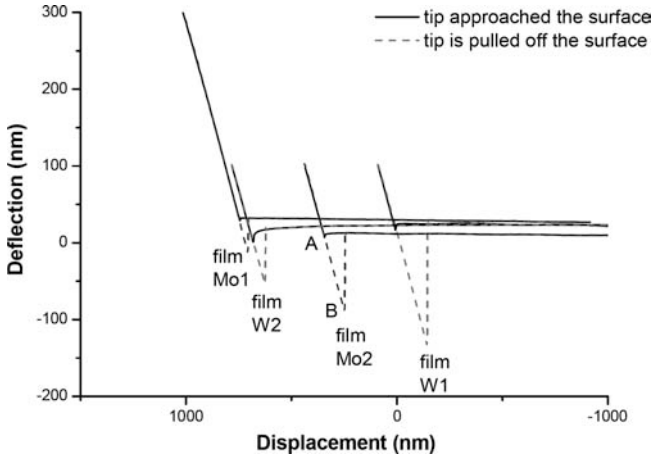

Fig. 5. Pull of force curves of the investigated films.

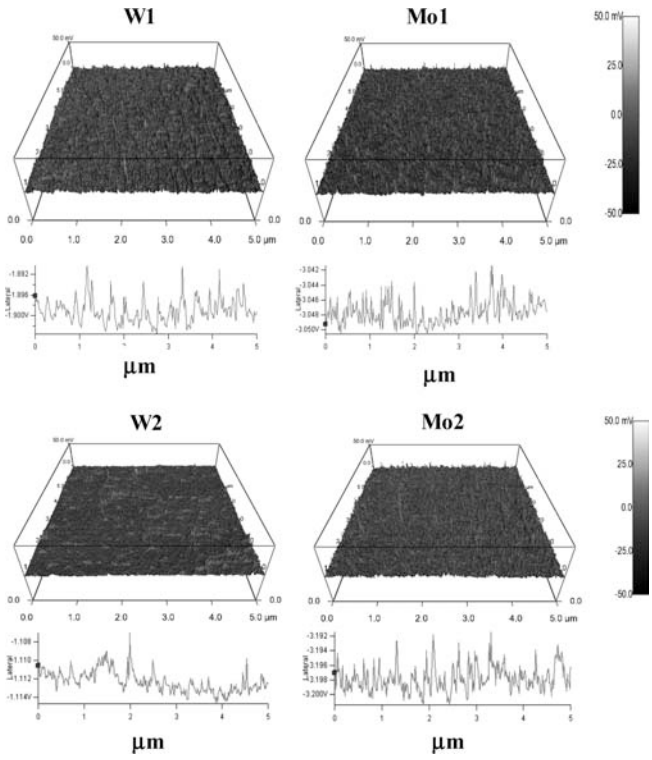

Fig. 6. Three-dimensional LFM images showing the friction surfaces of the investigated films together with representative cross-sectional line scans.

The three dimensional representations of the friction force values of these films are displayed in Fig. 6. These data were obtained for an applied load of 9 nN and a scan speed of 12.5 µm s^{-1}. The average friction force during forward scanning is higher than that during reverse scanning. The friction forces of various films are evaluated from the friction force values. The friction coefficients obtained using the procedure described above are presented in the form of a bar diagram in Fig. 7 for various films. Clearly friction coefficients of all films are quite low as estimated by AFM, a single asperity test. At low carbon content (35 at.%), W–S–C film has significantly lower friction coefficient than Mo–Se–C film. However, at higher carbon content friction coefficients of both films are comparable.

The relationship between RMS value (as obtained from topography) and the friction coefficient was studied. It is

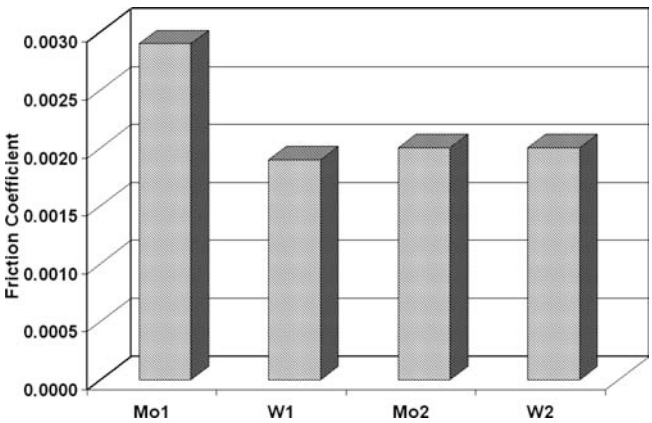

Fig. 7. Bar diagram showing the friction coefficient of the investigated films.

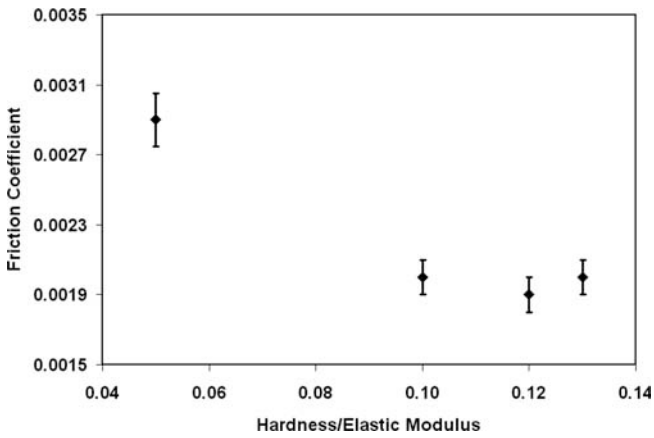

Fig. 8. The influence of mechanical properties on the friction coefficient.

clear that roughness does not have any clear effect on friction coefficient. The hardness and elastic modulus of two different types of films are so much different that establishing a direct correlation between friction coefficient and mechanical properties is not possible. However, the effect of hardness and elastic modulus on the friction coefficient can be obtained by noting the effect of the ratio of hardness to the elastic modulus (*H/E*) on friction coefficient. The variation of friction coefficient with *H/E* is given in Fig. 8. It appears that friction coefficient decreases with *H/E*.

4. Discussion

The key limitation of sharp tip AFM is poor repeatability from experiment to experiment primarily due to variation of tip geometry. That is why AFM is most useful when there is clear spatial and temporal variation of topography or lateral force. Despite this limitation, the present work has been able to clearly demonstrate superior friction properties of W–S–C film compared to Mo–S–C film at low carbon content. This work, however, could not differentiate friction properties of these two varieties of films at higher carbon content.

Although RMS surface roughness does not carry any information about slopes, sizes or frequencies of asperities, it is still an important parameter for predicting and understanding the properties of tribological systems. Earlier investigations indicated that friction coefficient of diamond film increases with increase in roughness [17, 18]. Higher roughness increases the asperities slope angle, which in turn increases the friction coefficient [17]. There are two mechanisms, which govern the roughness dependence of the friction coefficient. The first mechanism is known as ratchetting where relative motion between two surfaces is achieved by asperities riding over each other. The second possible mechanism is related to energy loss where asperities push each other. In the initial stage of sliding, there can be other operative mechanisms. The influence of roughness on the steady state friction coefficient in the present investigation does not show any direct relation. Thus the mechanisms mentioned above do not hold good for the present investigation. This may partly be related to the fact that the hardness and elastic modulus of W–S–C and Mo–Se–C films are widely different. Hence, they have

Table 5. RMS, Lateral correlation length and Hurst parameters of the investigated films.

Sample	AFM measure RMS (nm)	AFM measure RMS after flaterning on 0 level (nm)	σ – statistical RMS (nm)	ξ – lateral correlation length (nm)	α – Hurst parameter
Mo1	26.6	18	4.9	12.9	0.99
W1	18.2	13.4	4.3	12.5	0.99
Mo2	27.0	16.4	1.7	15.0	0.99
W2	29.8	20.6	7.8	37.4	0.99

different roughness dependence of friction coefficient. Also a different mechanism may play an important role in these systems.

The surface morphology of thin films can generally be described by a Gaussian self-affine fractal with a long wavelength cutoff. Such a model gives a surface height–height correlation function [19] of

$$C(r) = \sigma^2 \exp[-(|r|/\xi)^{2\alpha}] \quad (4)$$

where s is the root mean square amplitude of the surface or interface roughness. Parameter ξ is called the lateral correlation length. The correlation length is a measure of and denotes the average length for which the heights between two surface points are correlated. ξ is a measure for the lateral fluctuations of the roughness. The third parameter is the roughness exponent α, also called Hurst parameter, which is related to the local fractal dimension d of the surface through $\alpha = 3 - d$. It tells how jagged a surface with a given rms roughness and lateral correlation length is. α usually ranges between 0.5 (exponential decay of $C(r)$-more jagged surface) and 1 (Gaussian $C(r)$-less jagged). There are easy ways to determine these three roughness parameters from a given morphology: These parameters as determined for the investigated surfaces are listed in Table 5. Clearly lateral correlation length follows the same trend as that of RMS values of the as received surfaces confirming the above discussion on friction coefficient and surface roughness. Hurst parameters also indicate that the surface is less jagged for the given surface roughness.

The roughness parameters of the films are around 18 to 30 nm (RMS). W–S–C films have low roughness compared to Mo–Se–C films. The maximum depth of indentation at 2 mN load is around 118 nm for W–S–C films and between 187 nm (Mo2) to 264 nm (Mo1) for Mo–Se–C films. Thus maximum depth of indentation is around 8 times the roughness (RMS). Further, the thickness of the W–S–C film is 1 000 nm for W1 film and 2 000 nm for W2 film. The thickness of Mo2 film is 2 000 nm and that of Mo1 film is 3 000 nm. This indicates that the film thickness is nearly 10 times the maximum depth of indentation. The indentation process fulfills the roughness criteria and film thickness criteria. Thus, hardness measurement is a valid indentation process and the hardness obtained is representative of true hardness of the film. At this stage it should be stated that the roughness (RMS) value reported in this work is rather high as the film thickness is 1 000 nm and above. For most of the MEMS application required film thickness is an order of magnitude lower. As reported previously [20], the roughness of a film decreases as the thickness of the film decreases.

Figure 5 clearly indicates that for both varieties of film pull off force decreases with increasing carbon content. This fact, the increase in pull-off force with decrease in carbon content may be related to a decrease in oxygen adsorption on the surfaces. These values are substantially lower than the pull-off force calculated to be 445 nN for Ti/*a*-C : H film and lower than the pull off force of 76.4 nN plasma enhanced chemical vapour deposited (PECVD) diamond film reported earlier [21]. Further, it can be noted that pull-off force follows a trend of W2 < A2 < Mo2 < Mo1. However, friction coefficient does not follow a similar trend. When W–S–C or Mo–Se–C systems are considered separately, friction coefficient and pull-off force follows the opposite trend for the W–S–C system whereas it follows a similar trend Mo2 < Mo1 for the Mo–Se–C system. Thus, adhesion is not directly related for the W–S–C system and it may be related for the Mo–S–C system.

Recently it was demonstrated that not only hardness and elastic modulus but also the ratio *H/E* is very important materials properties [22]. The ratio *H/E* multiplied by a geometric factor, which is the ratio of the diameter of the plastic zone to total deformed zone, gives the plasticity index. The plasticity index describes the deformation properties of contacting surfaces. This quantity also appears in various expressions for fracture toughness. In the present work, though the hardness and elastic modulus of W–S–C films were significantly higher than those of Mo–Se–C films, the ratios of *H/E* are comparable. Thus the present work clearly indicates that as long as this ratio (*H/E*) is high, friction coefficient will be low.

The applied load during AFM study is very low. The wear under such condition can be negligible. There are two important friction dissipation mechanisms under this no wear condition. The first mechanism is dissipation of friction energy by emission of phonons [23]. The second mechanism is dissipation of friction energy by electron hole pair excitation [24]. To date it is not clear which mechanism dominates. Some authors have proposed that the electronic mechanism is the important mechanism for friction dissipation. As the carbon content is increased, sp^2 hybridisation increases. Hence a similar electronic behaviour is expected for both varieties of films (e. g. for W–S–C and Mo–Se–C films) with increase in carbon content. Since W–S–C and Mo–Se–C films exhibit different friction response with carbon content, the electronic mechanism cannot be considered to be dominant mechanism. In that case phononic emission can be considered to be the dominant mechanism. Further, phononic emission is usually considered to be the dominant mechanism in insulating systems and the films investigated in present work are insulating materials.

Finally it is noted that the hardness and elastic modulus of W–S–C film are considerably higher than those of Mo–Se–C films. Further, hardness and elastic modulus of W–S–C based films are insensitive to carbon content even though film with low carbon content has low roughness (RMS). As the friction coefficient decreases with increase

in the ratio of hardness to elastic modulus, it is clear that film W1, i.e. the W–S–C film with low carbon content, exhibits the best combination of hardness, elastic modulus, friction coefficient and roughness. Thus film W1 is the best-suited self-lubrication film among the films investigated in present work for nanotribological application.

5. Conclusions

1. The roughness parameter indicated by the RMS value is higher for Mo–Se–C film than W–S–C film at low carbon content and at high carbon content W–S–C film has a higher RMS value than Mo–Se–C film.
2. Carbon content of the investigated films influenced pull-off force values. Further, Mo–Se–C films have higher pull-off force than W–S–C films.
3. The friction coefficient of Mo–Se–C film at this low load range decreases with increasing carbon content. However, for W–S–C films the friction coefficient is independent of carbon content.
4. Friction coefficient of all these films decreases with increasing *H/E* ratio.

The authors are grateful to Prof. A. Cavaleiro and his group, University of Coimbra for providing the test materials. The authors are also grateful to the European Commission for supporting this work through their project no MIMO1-CT-2006-039220 and WEMESURF research-training network. The authors also sincerely acknowledge the excellent review and suggestions of the reviewers.

References

[1] R. Bichel, F. Levy: Thin Solid Films 116 (1984) 125.
[2] A. Malloucky, J.C. Bemede: Thin Solid Films 158 (1988) 285. DOI:10.1016/0040-6090(88)90032-6
[3] A. Jager-Waldau, M. Lux Steiner, R. Jager-Waldau, R. Burkhardt, E. Bucher: Thin Solid Films 189 (1990) 330.
[4] J. Wang, W. Lauwerens, E. Wieers, L.M. Stals, J. He, J.P. Celis: Surf. Coat. Technol. 139 (2001) 143. DOI:10.1016/S0257-8972(01)00988-4
[5] V.Y. Fomsinky, R.I. Romanov, A.V. Gusarov, J.P. Celis: Surf. Coat. Technol. 201 (2007) 7813. DOI:10.1016/j.surfcoat.2007.03.006
[6] T. Kubart, T. Polkar, L. Kopecky, R. Novak, D. Novakova: Surf. Coat. Technol. 193 (2005) 230. DOI:10.1016/j.surfcoat.2004.08.146
[7] D.V. Shtansky, T.A. Lobova, V.Yu Fominski, S.A. Kulinich, I.V. Lyasotsky, M.I. Petrzlük, E.A. Levashow, J.J. Moore: Surf. Coat. Technol, 183 (2004) 328. DOI:10.1016/j.surfcoat.2003.09.047
[8] A. Nossa, A. Cavaleiro: Surf. Coat. Technol., 142 – 144 (2001), 984.
[9] A. Nossa, A. Cavalerio: J. Mater. Res. 19 (2004) 1. DOI:10.1557/JMR.2004.0293
[10] T. Polcar, M. Evaristo, A. Cavaleiro: Surf. Coat. Technol, Synthesis and structural properties of Mo–Se–C sputtered coatings, in press.
[11] W.C. Oliver, G.M. Pharr: J. Mater. Res. 7 (1992) 1564. DOI:10.1557/JMR.1992.1564
[12] B. Bhushan, Principles and Applications of Tribology, ISBN 0–471-59407–5, John Wiley & Sons, New York, USA, 1999.
[13] B.D. Beake, I.U. Hassan, C.A. Rego, W. Ahmed: Diamond and Rel. Mater. 9 (2000)1421. DOI:10.1016/S0925-9635(00)00251-X
[14] J. Ding, Y. Meng, S. Wen: Thin Solid Films 371 (2000) 178. DOI:10.1016/S0040-6090(00)01004-X
[15] G. Weise, N. Mattern, H. Hermann, A. Teresiak, I. Bacher, W. Bruckner, H.D. Bauer, H. Vinzelberg, G. Reiss, U. Kreißig, M. Mader, P. Markschlager: Thin Solid Film 298 (1997) 98. DOI:10.1016/S0040-6090(96)09165-1
[16] T. Koch, M. Evaristo, A. Pauschitz, M. Roy, A. Cavaleiro: Thin Solid Film 518 (2009) 185. DOI:10.1016/j.tsf.2009.06.027
[17] S.J. Bull, P.R. Chalkar, C. Johnston, V. Moore: Surf. Coat. Technol. 68 (1994) 603. DOI:10.1016/0257-8972(94)90224-0
[18] S.E. Grillo, J.E. Field: J. Phys. D: Appl. Phys. 30 (1997) 202. DOI:10.1088/0022-3727/30/2/007
[19] S.K. Sinha, E.B. Sirota, S. Garoff, H.B. Stanley: Phys. Rev. B 38 (1988) 2297. DOI:10.1103/PhysRevB.38.2297
[20] S. Kavasnica, J. Schalko, C. Eisenmenger–Sittner, J. Bernardi, G. Vorlaufer, A. Pauschitz, M. Roy: Diamond Rel. Mater. 15 (2006) 1743. DOI:10.1016/j.diamond.2006.03.005
[21] A. Pauschitz, J. Schalko, T. Koch, C. Eisenmenger–Sittner, S. Kvasnica, M. Roy: Bull. of Mater. Sci. 26 (2003) 585. DOI:10.1007/BF02704320
[22] J. Musil, M. Jirout: Surf. Coat. Technol. 201 (2007) 5143. DOI:10.1016/j.surfcoat.2006.07.020
[23] M. Cieplak, E.D. Smith, M.O. Robbins: Science 265 (1994) 1209. DOI:10.1126/science.265.5176.1209 PMid:17787586
[24] B.N.J. Persson: Phys. Rev. B 44 (1991) 3277. DOI:10.1103/PhysRevB.44.3277

(Received January 18, 2009; accepted April 27, 2010)

Bibliography

DOI 10.3139/146.110358
Int. J. Mat. Res. (formerly Z. Metallkd.)
101 (2010) 7; page 845 – 851

ISSN 1862-5282

Correspondence address

Prof. Ille C. Gebeshuber
Institut für Angewandte Physik
Technische Universität Wien
Wiedner Hauptstraße 8 – 10/134
1040 Wien, Austria

Institute for Microenergineering and Nanoelectronics
Universiti Kebangsaan Malaysia
43600 UKM Bangi, Malaysia
Tel.: +60 12 392 92 33 (Malaysia)
+43 664 350 7654 (Austria)
Fax: +60 380 620 183 (Malaysia)
+43 158 801 134 99 (Austria)
E-mail: gebeshuber@iap.tuwien.ac.at
ille.gebeshuber@mac.com